JOURNAL OF MATERIALS SCIENCE 24 (1989) 3029–3039

# Dissolution shapes of *Y*-rotated quartz plates and *Y* sections derived from the polar diagram of the dissolution slowness

C. R. TELLIER, T. G. LEBLOIS, P. C. MAITRE
*Laboratoire de Chronométrie, Electronique et Piézoélectricité Ecole Nationale Superieure de Mecanique et des Microtechniques Route de Gray, La Bouloie, 25030 Besancon Cedex, France*

A study has been made of the rate at which various *Y*-rotated quartz plates are etched in a concentrated ammonium bifluoride solution. The changes in the surface texture of these differently oriented plates on repeated etching are systematically investigated. To obtain all the information needed for an analysis of the dissolution shapes in the framework of the tensorial representation of the dissolution slowness the profile graph of a deeply etched *Y*-cut plate is also reported. The polar diagram $L_{XZ}(\theta)$ of the dissolution slowness associated with the *Y*-rotated quartz plates is then derived using profile graph data. Numerical and graphical simulations of the dissolution shapes are used to verify the adequation of the law $L_{XZ}(\theta)$. The comparison of the theoretical etch profiles with the $Z''$ etch profiles produced by repeated etching on some *Y*-rotated quartz plates shows complete agreement. Excellent agreement is also found between the theoretical and experimental shapes of the magnified profile graph related to deeply etched *Y* sections. From the consistency between the observed dissolution shapes and the computed shapes deduced from the tensorial analysis of the dissolution we can conclude that the proposed polar diagram $L_{XZ}(\theta)$ represents accurately the variations of the dissolution slowness with the angle $\theta$ in the *XZ* plane.

## 1. Introduction

Interest in chemical etching as a procedure to prepare high-frequency quartz resonator plates [1–14] with clean and smooth surfaces has been revived in the past few years. The possibility of a chemical polishing of quartz surfaces by immersion in $NH_4HF$ solutions or in $NH_4F$ with HF mixture has been investigated and some satisfactory results have been obtained on AT-cut [1, 2, 7, 8] and SC-cut [5, 6, 14] quartz plates. However some experiments on differently oriented quartz plates [10, 11, 14–17] provided evidence for a formation of final dissolution figures whose shape depends on the crystal orientation in agreement with other works [18–21] which outlined that the etch pits invariably bear some symmetry with the crystal surface. Discussing their experimental results Tellier *et al.* [22, 23] states that the shape of dissolution figures can be understood in terms of the kinematic model [24–26] originally given by Lighthill and Whithan [25] and a numerical simulation of the dissolution profiles developed. In particular these authors [27] showed that it is possible to determine the trajectory of a moving surface profile element using a vectorial analysis where the dissolution is described in terms of an orientation dependent dissolution slowness vector, $\vec{L}$. Recently Tellier *et al.* [28] developed an analysis in three dimensions where, as the orientation of the moving surface element varies, the extremity of the dissolution slowness vector lies at different points of the representative slowness surface. They used a tensorial method to determine, for quartz crystal, the equation of the representative surface of the dissolution slowness vector and taking into account the symmetry of quartz crystal to reduce the number of dissolution constants they proposed a generalized equation for the slowness surface. Some unknown coefficients appearing in this general equation were determined using experimental results on the dissolution rate of singly rotated quartz plates (Fig. 1) and a very satisfactory agreement was observed between theoretical and experimental results [28]. The present work continues along this line and presents results on the anisotropic geometrical features of *Y*-rotated quartz plates ($\Psi = (\pi/2, \theta)$) caused by chemical etching. These results are discussed in the framework of the tensorial representation of the dissolution in order to derive in the $(x, z)$ plane the polar diagram of the slowness vector, $\vec{L}$. Using a numerical simulation of the dissolution profiles and of the dissolution shape of sections a systematic comparison of the theoretical and experimental shapes is undertaken.

## 2. Experimental procedures

The resonators used here were doubly-rotated plano-convex quartz plates. Since $\Psi = 90°$ and only $\theta$ varies these plates are readily identified with *Y*-rotated

0022–2461/89 $03.00 + .12 

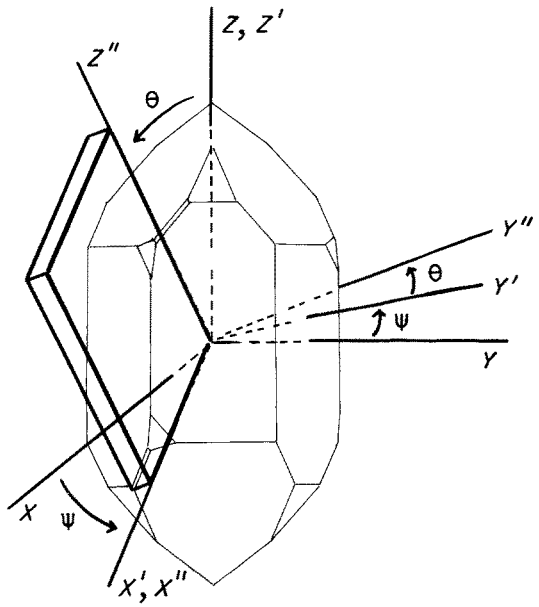


*Figure 1* Doubly rotated plates of quartz crystals.

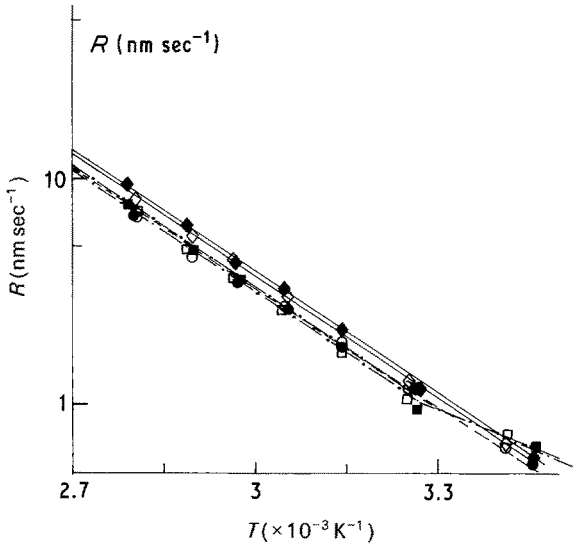


*Figure 2* Plot of ln $R$ against $T^{-1}$ for various $Y$-rotated quartz plates (◇) $Y$-45 plate ($\theta = +45°$); (◆) $Y$-45* plate ($\theta = -45°$); (●, ○) $Y$-35 plates ($\theta = 35°$); (■, □) $Y$-55 plates ($\theta = 55°$).

quartz plates. The plates with the angle $\theta$ respectively equal to 35, 45, 55 and $-45°$ and labelled for convenience $Y$-35, $Y$-45, $Y$-55 and $Y$*-45 were cut from a single synthetic quartz crystal. Before the plates were etched they were lapped with a 5 $\mu$m abrasive. The plates were initially of circular shape with a 13.2 mm diameter.

These plates were etched in a concentrated ammonium bifluoride solution at a constant temperature in the range 290–360 K for various periods of time. The etching procedure has been described elsewhere [8].

The topography of the two surfaces of the various quartz plates was studied by means of two different procedures. Firstly, the surface profiles were characterized at any time of etching by using a microprocessor-based surface profilometer. In particular the traces were made along directions which coincide with the $Z''$ direction. Secondly, after each isothermal etching, scanning electron microscopy (SEM) studies were carried out on these non-conducting specimens by using a low accelerating voltage (1 kV) and an observation angle of 0°. In addition final SEM micrographs were taken from the backscattered electron topographic image of deeply etched quartz plates.

The changes in roughness of the circular starting shape of $Y$ sections were studied by using a Talyrond analyser which generates the least square circle so that the dissolution profiles were displayed at relatively large magnifications with the superimposed reference circle. A flat mark was machined on the circular edge of all resonators which made easy to locate at $\pm 0.25°$ the $X$ axis during the various form and surface texture measurements.

## 3. Results

### 3.1. Dissolution rate of $Y$-rotated quartz plates

Decrements in thickness, $\Delta d$, were evaluated from frequency measurements by means of the well-known formula [29]

$$\Delta d = -K \frac{\Delta f}{f_i f_f} \quad (1)$$

where $f_i$ and $f_f$ are the initial and final frequencies and $\Delta f$ the change in the resonance frequency caused by chemical etching. The constant $K$ depends on the overtone of the thickness–shear mode vibration and on the orientation of the quartz plate.

Assuming that during isothermal etchings the decrement in thickness, $\Delta d$, varies linearly with the etching time $t$, as frequently observed [8, 9, 16] for differently oriented quartz plates, average values of the dissolution rate, $R$, were evaluated for successive intervals of the etching time. The data are plotted (Fig. 2) in the form ln $R$ against $1/T$ according to the well-known Arrhenius equation [30]:

$$R = A \exp\left(-\frac{E_a}{K_B T}\right) \quad (2)$$

where $k_B$ is the Boltzmann constant, $E_a$ is an apparent activation energy and $T$ is the absolute temperature. The pre-exponential term $A$ includes concentration terms. The data are approximately fitted by straight lines except for the $Y$-55 cuts where the knee which occurs in the low temperature region can be understood in terms of an enhancement of the etch rate due to the strained surface layer created by mechanical lapping. Clearly the activation energy, $E_a$, as evaluated in the high temperature region is almost independent of the crystal orientation. Moreover in the high temperature region the influence of the crystal orientation on the etch rate remains very slight in apparent contradiction with previous results [11, 14, 16, 17] on singly rotated quartz plates for which large changes in the etch rate with the crystal orientation have been observed.

### 3.2. Surface texture of $Y$-rotated quartz plates

In this work we investigated the changes in the $Z''$ surface profilometry traces with the average depth of etch, $\Delta d_S \simeq \Delta d/2$, of a resonator surface. They are two interesting features of this study which can be summarized as follows.

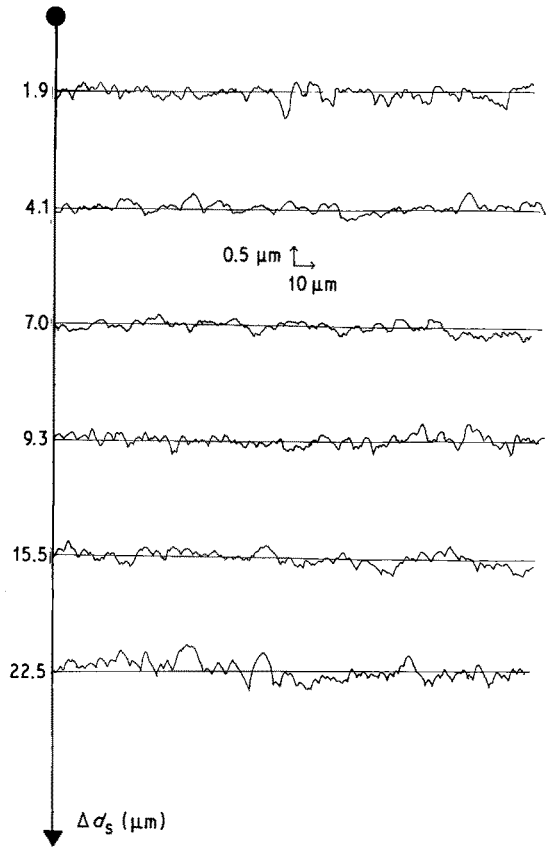


*Figure 3* Changes in the surface profilometry traces with the depth $\Delta d_s$ of etch of an *Y*-35 plate. The traces are made along the *Z″* direction and on the planar face of the resonator.

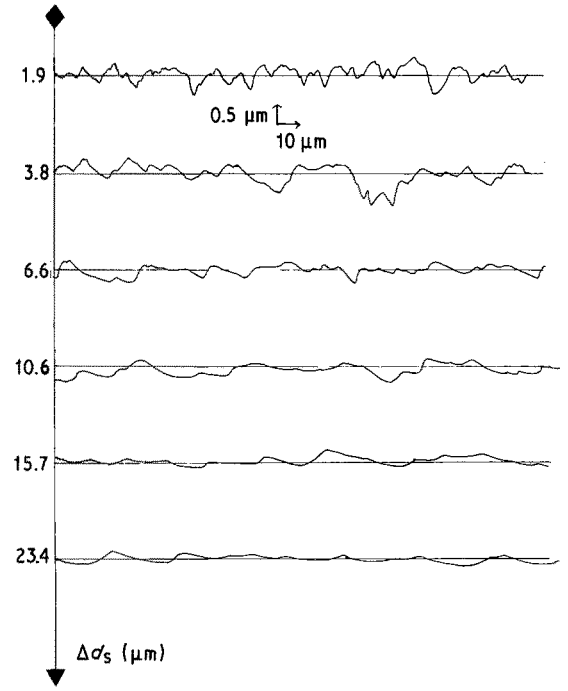


*Figure 4* Changes in the profilometry traces made along the *Z″* direction of the planar face of an *Y*-55 plate.

1. The *Z″* traces made on a given planar or convex surface have markedly oriented changes on etching. This behaviour is particularly typified by the *Z″* profilometry traces made on the planar surface of the *Y*-35 and *Y*-55 plates (Figs 3 and 4). The final *Z″* profile related to the *Y*-35 planar surface is readily identified as convex where as *Z″* profiles of alternate convex-concave shape develop on the planar *Y*-55 surface. Moreover the etching produces more elongated *Z″* profiles on the *Y*-55 surface than on the *Y*-35 surface.

2. For a given plate we observe differences (Fig. 5) in the final shape of the *Z″* traces made on the two surfaces of the deeply etched plate ($\Delta d_S > 10\,\mu m$). This orientation effect is particularly evident for the *Y*-55 plate for which very distinctive shape of *Z″* profiles are characterized on the two surfaces and for which subsequent etching results in a markedly elongation of the final *Z″* profiles for only one of the two surfaces. This last observation is still adequate for *Y*-35 and *Y*-45 plates even if the difference between the waviness spacing of the two *Z″* profilometry traces is less pronounced than for the *Y*-55 plate. It should be also remarked that only the shape of *Z″* traces made

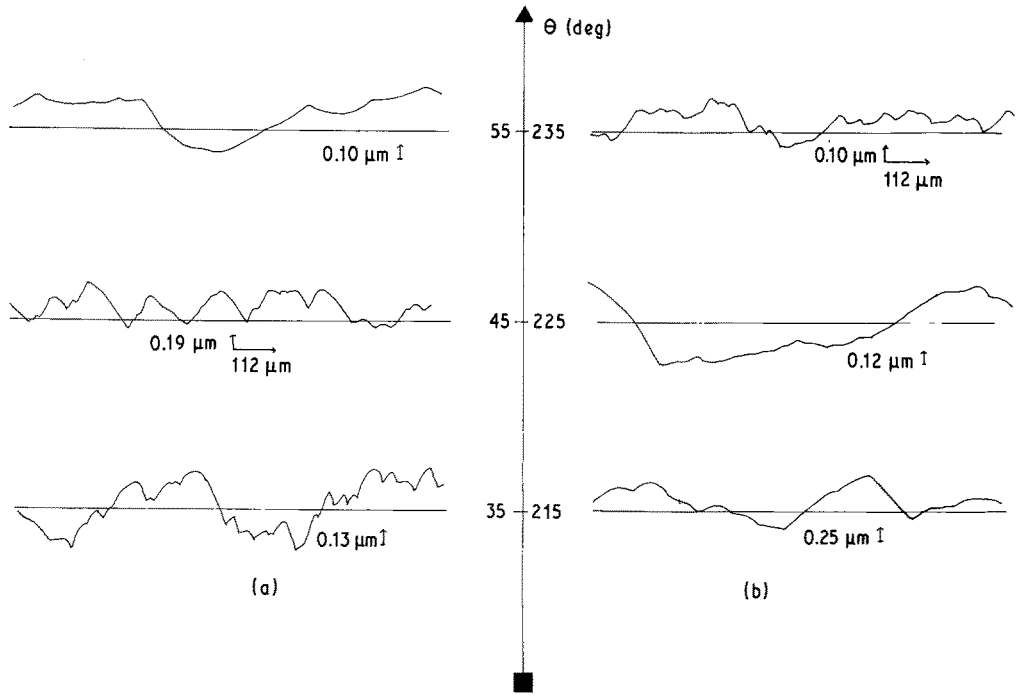


*Figure 5* The final *Z″* profilometry traces made on (a) the planar and (b) the convex face of differently oriented *Y*-rotated plates.

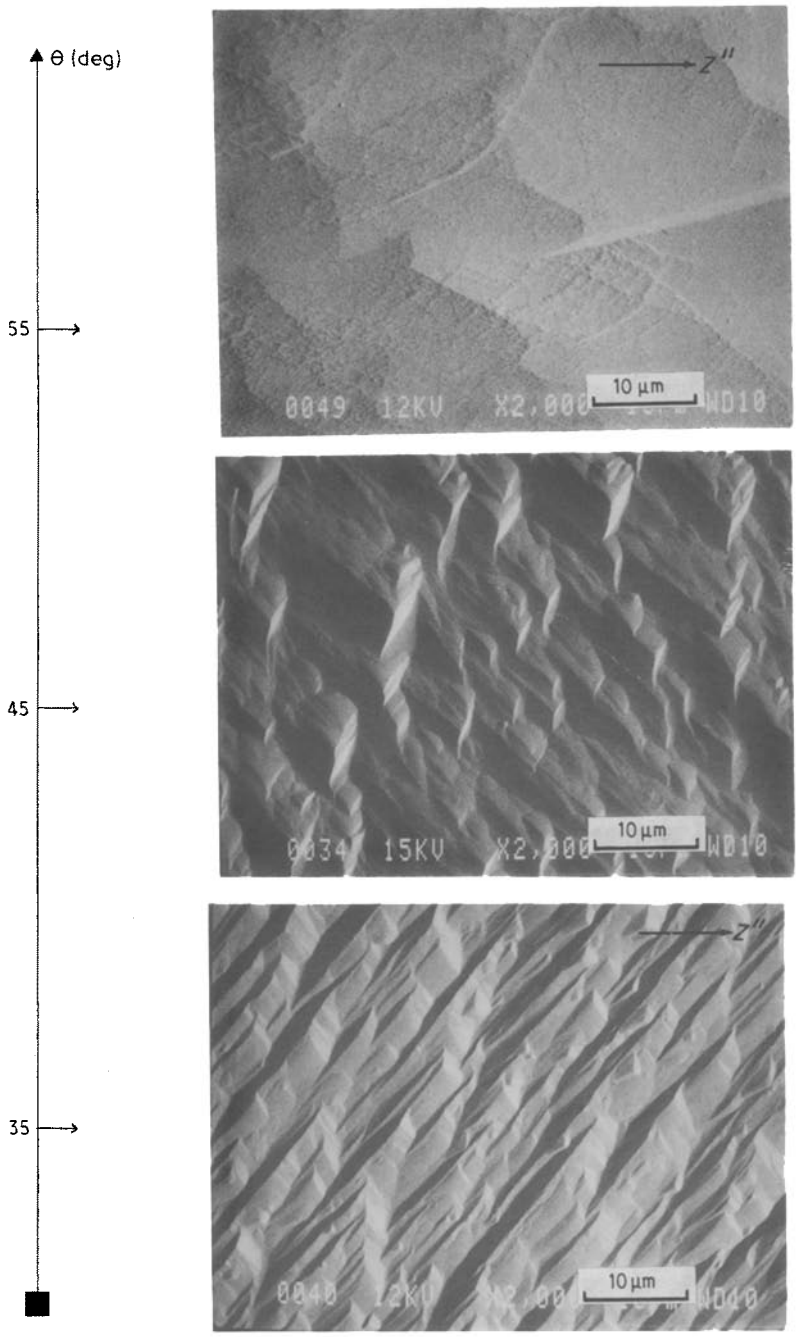


*Figure 6* SEM micrographs of the planar face of various deeply etched *Y*-rotated quartz plates.

only the convex *Y*-45 surface remains rather undefined and cannot be distinctly qualified of convex or concave.

The final SEM micrographs (Figs 6 and 7) of the two surfaces reveal also typical and uniformly shaped etch figures. The figures produced on the convex face of the deeply etched *Y*-rotated plates are essentially different from those formed on the other face. The orientation of the dissolution figures which remains uniform for a given face appears also to be a characteristic of the face orientation.

### 3.3. The dissolution shape of the *Y* section

The final dissolution profile of the *Y*-plate is shown in Fig. 8 at a moderate 200 magnification choosing the least squares circle as a reference. At this magnification the out-of-roundness presents successive maxima and minima corresponding to specific directions lying in the $(x, z)$ plane. The values of the angle, $\beta$, that these directions make with the crystallographic *X* axis can be determined with an accuracy of about 1°. It should be pointed out that the marked out-of-roundness in the vicinity of the *X* direction is due to the initial flat mark. Inevitably this mark generates a large roundness error which can be easily distinguished on the profile graph. However the most interesting feature revealed by Fig. 8 is that the profile graph can be divided in two parts with respect to the *X*-direction, one of which is the mirror image of the other. So that similar extrema occur for opposite values $\pm\beta_i$ of the angle $\beta$.

## 4. Theoretical considerations

### 4.1. The polar diagram of $\vec{L}$ for *Y*-rotated quartz plates

Let us recall that in a kinematic analysis of the dissolution it is convenient in three dimensions $(x, y, z)$ to introduce a vector associated with a moving surface element ds of orientation $(\Psi, \theta)$ in such a way we are able to track easily the movement of the surface element within the crystal during the dissolution. This

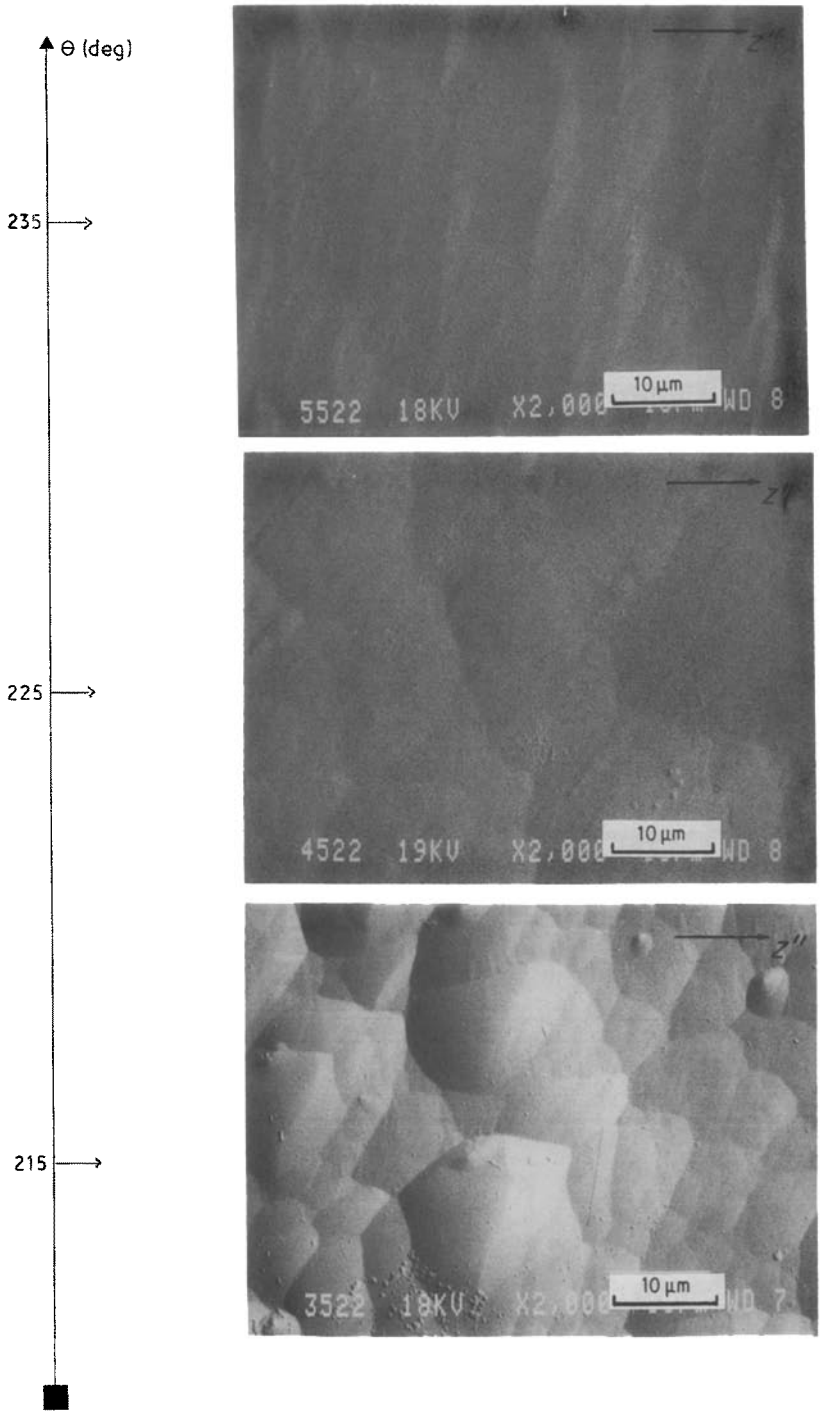


*Figure 7* SEM micrographs of the convex face of various deeply etched *Y*-rotated quartz plates.

vector is found to be [28] the dissolution vector, $\vec{L}$, whose magnitude, $L$, is the reciprocal of the normal dissolution rate, $v_N$, and whose positive direction coincides with that of the inward normal unit vector, $\vec{n}$, to the surface element (Fig. 9). As the orientation ($\Psi$, $\theta$) varies the extremity of the slowness vector, $\vec{L}$, lies at different points of the representative slowness surface. Here we adopt the system of notation specified in the IEEE standard on piezoelectricity [31] where two rotations suffice to define the orientation of the surface element, the first rotation of amount $\Psi$ is about the crystallographic $Z$ axis while the second rotation of amount $\theta$ is about the crystallographic $X$ axis (Fig. 1) so that the cartesian components of the inward normal, $\vec{n}$, to the surface element are given by

$$n_x = \sin \Psi \cos \theta, \quad n_y = -\cos \Psi \cos \theta,$$
$$n_z = -\sin \theta \tag{3}$$

Using a tensorial representation of the dissolution slowness we have previously shown [28] that the equation of the representative surface involving the three components of $\vec{n}$ can be expressed in terms of dissolution tensors. Then taking into account the restriction on the dissolution constants due to the crystal symmetry for tensors up to the 16th order it becomes possible to propose a general relation

$$L = L_0 + \sum_{j=1}^{m} A_j \cos^{2j} \theta + \sum_{k=1}^{n} B_k \cos^{2k+1} \theta \sin 3\Psi + \sum_{l=1}^{n} C_l \cos^{2l+1} \theta \sin \theta \cos 3\Psi \tag{4}$$

which gives the magnitude, $L$, of the dissolution slowness vector for all possible values of the angles $\theta$ and

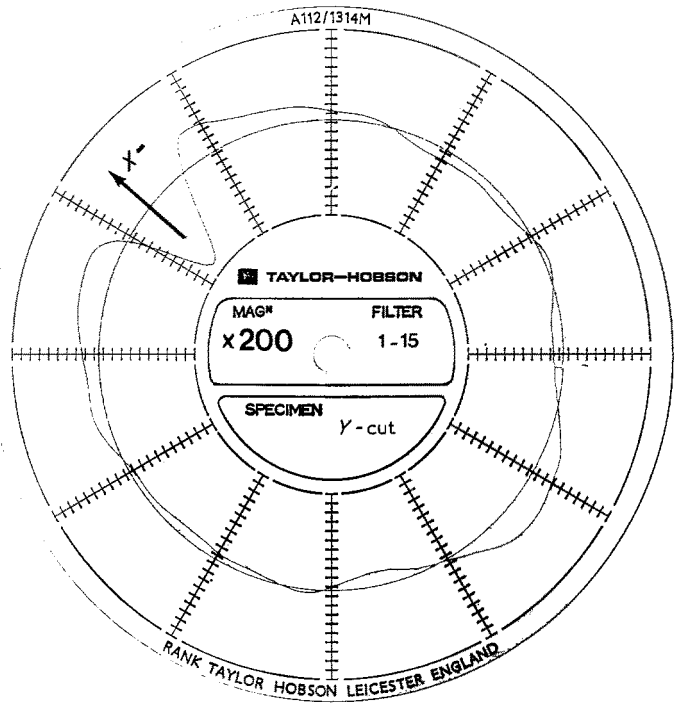


*Figure 8* A magnified (× 200) profile graph of a deeply etched $Y$ section ($\Psi = 0°$, $\theta = 0°$).

$\Psi$ and thus constitutes the equation of the representative slowness surface.

For $Y$-rotated cuts defined by $\Psi = 90°$ and by successive values of the angle $\theta$ the slowness dissolution vector, $\vec{L}$, related to any two faces of the various cuts lies in the $(X, Z)$ plane and makes an angle $\beta$ with the $X$ axis whose value, depending on the face into consideration, is found to be equal to $\theta$ or to $\theta + 180°$. Let us consider the various faces corresponding to the $\theta$ value; for these faces the polar diagram of the slowness vector takes the form

$$L_{XZ}(\theta) = L_0 + \sum_{j=1}^{m} A_j \cos^{2j}\theta - \sum_{k=1}^{n} B_k \cos^{2k+1}\theta \tag{5}$$

where the unknown constants $L_0$, $A_j$ and $B_k$ which are expressed in terms of the dissolution constants are to be evaluated from experimental measurements.

Turning our attention to the normal dissolution rate it appears from the above considerations that the normal dissolution rate, $v_N$, differs for the two faces of an $Y$-rotated resonator of orientation ($\Psi = 90°$, $\theta = \theta_1$) according to the relations

$$v_{N1} = \left[L_{XZ}(\theta = \theta_1)\right]^{-1} \tag{6}$$

$$v_{N2} = \left[L_{XZ}(\theta = \theta_1 + 180°)\right]^{-1} \tag{7}$$

which hold for the face 1 and the face 2 of the resonator, respectively.

Thus the etch rate introduced in Section 3.1 whose values are deduced from Arrhenius plots of the etch rate against $1/T$ constitutes only an average etch rate defined as

$$R = \frac{v_{N1} + v_{N2}}{2} \tag{8}$$

In these conditions a complete set of data on the etch rate does not permit to identify the true values of $L_{XZ}(\theta)$ and $L_{XZ}(\theta + 180°)$ and consequently to evaluate the unknown constants appearing in Equation 5. This evaluation requires an alternative experimental procedure. For this purpose, let us note that the mechanical processes which produce resonators with a starting circular shape creates on the resonator edge a disturbed layer whose thickness can be estimated to be close to 15 $\mu$m. Thus as soon as the decrease in diameter reaches 30 $\mu$m the further decrease due to subsequent etching can be solely attributed to the anisotropic etching of quartz crystal. Thus profile graphs of deeply etched $Y$ sections can at large magnifications, yield approximate values of the

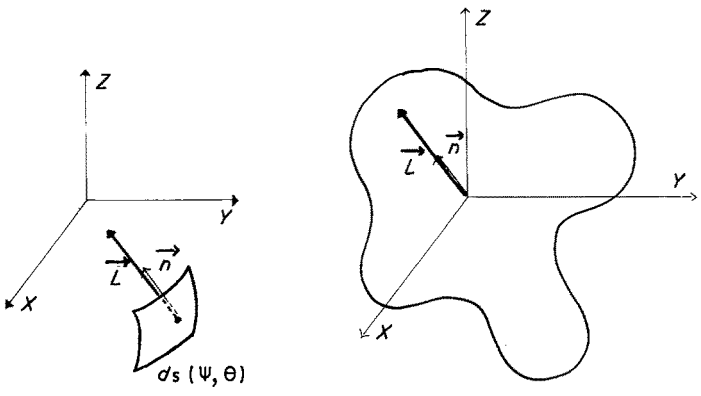


*Figure 9* Representation of the dissolution slowness vector, $\vec{L}$, and of the slowness surface in a three-dimensional model.

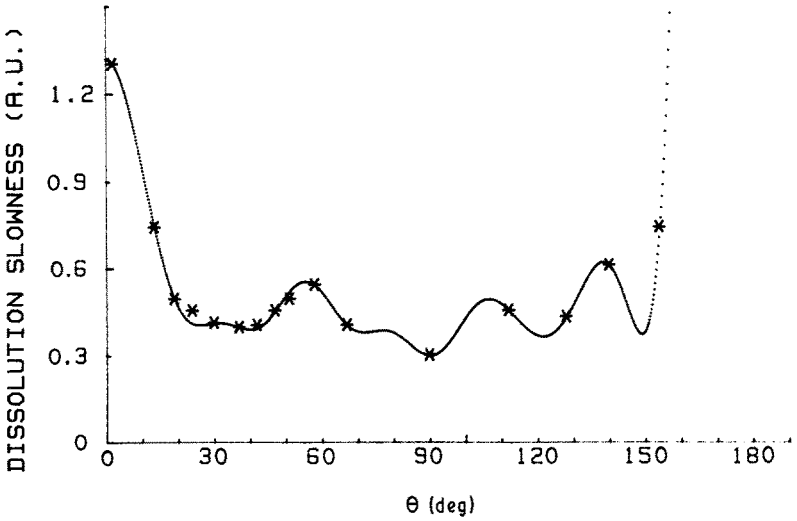


*Figure 10* Variations of the dissolution slowness $L_{XZ}$ against the angle $\theta$. The dotted line corresponds to the theoretical plot. (★) data as evaluated from the profile graph of a deeply etched $Y$ section.

dissolution slowness $L_{XZ}(\theta)$ related to a single face of the resonator. A tentative to evaluate the unknown constants $L_0$, $A_j$ and $B_k$ by means of this procedure was undertaken. The result is illustrated in Fig. 10 where the plot $L(\theta)$ against $\theta$ as derived from the theoretical Equation 5 by introducing constants evaluated up to the 14th order fits remarkably well data for angles $\theta$ in the range 0 to 180°.

## 4.2. Numerical simulation of dissolution shapes

To establish the consistency of the present model and

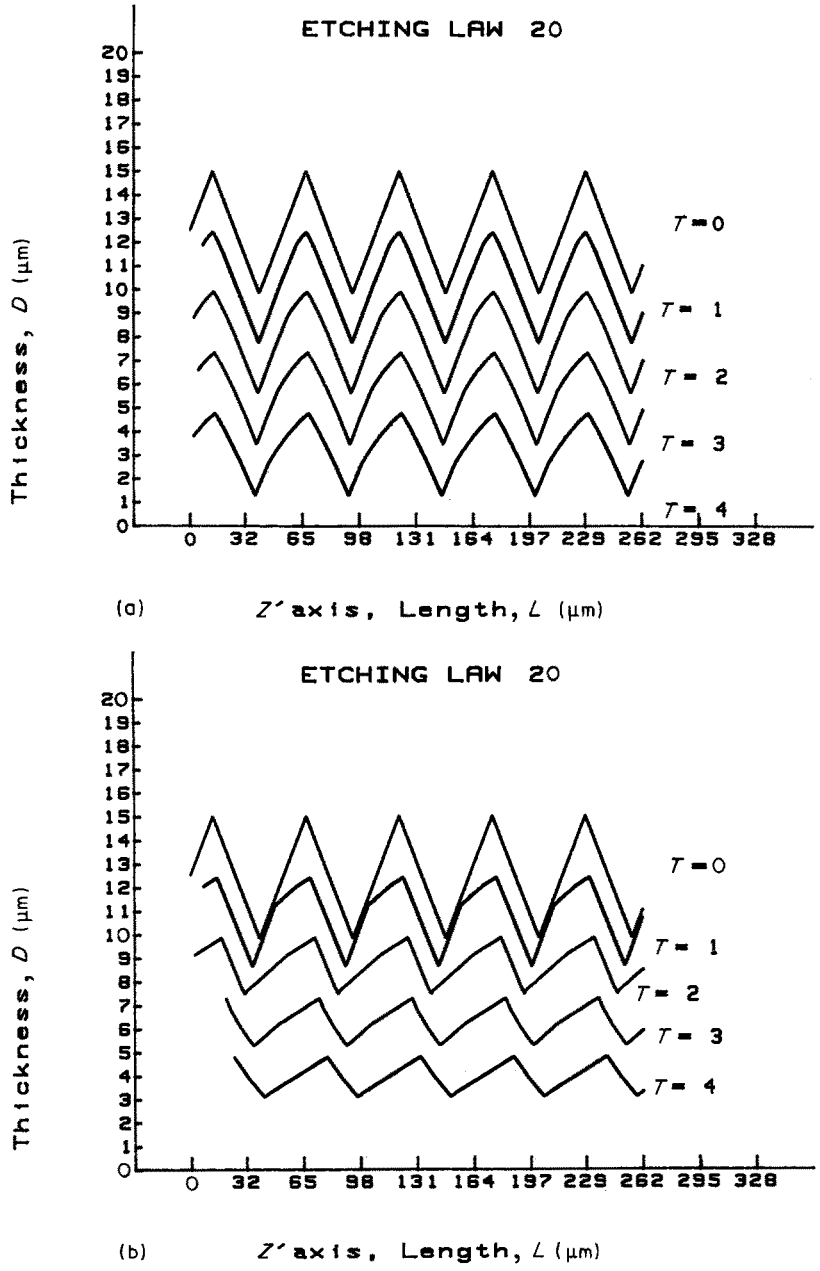


*Figure 11* The theoretical changes in the shape of an initial triangular surface profile. The case of an $Y$-35 plate; (a) the planar face ($\theta$ = 35°); (b) the convex face ($\theta$ = 145°).

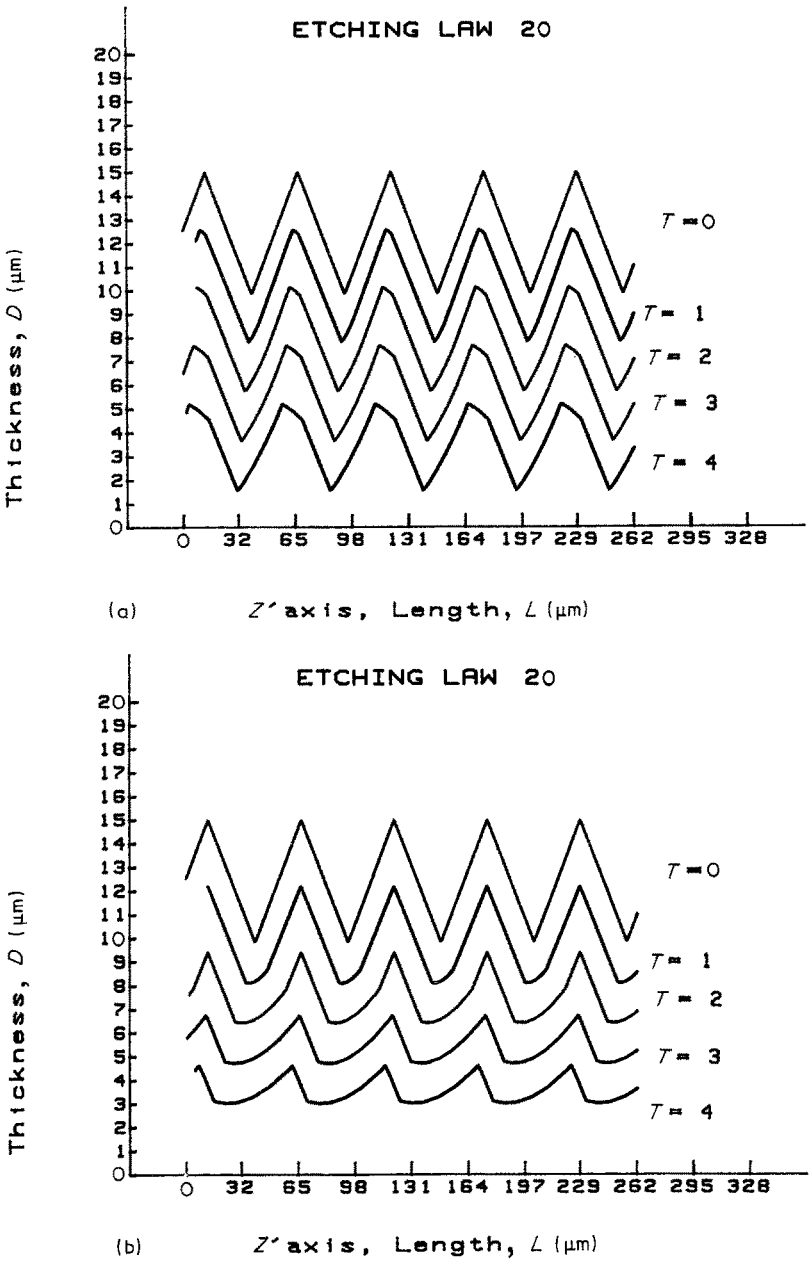


*Figure 12* As Fig. 11 for an *Y*-45 plate; (a) the planar face ($\theta = 45°$); (b) the convex face ($\theta = 135°$).

to verify the adequation of the preceding experimental evaluation of constants $A_j$, $B_k$ and $L_0$ we have to investigate theoretically two different types of information on the geometrical aspects of etched *Y*-rotated quartz plates directly derived from the polar diagram of $L_{XZ}(\theta)$:

1. given a particular starting cut we can follow graphically the evolution of the shape of $Z''$ profiles with increasing etching times [20, 21, 28];

2. given a circular starting shape we are able to deduce successive dissolution shapes of the *Y* section of quartz crystals from the polar diagram.

A numerical simulation has been previously developed [19, 20, 28] to track the changes in shape of dissolution profiles. The program which was described elsewhere [19, 20] was modified to construct in two dimensions the dissolution shapes of sections for the case of either a spherical hollow or a sphere of crystal. It now calculates the trajectory of a moving surface element tangent at a given point on the initial spherical surface and here again it eliminates section elements whose trajectories are found to meet during the dissolution.

Theoretical results on the formation of the $Z''$ dissolution profiles are collected in Figs 11 to 13. Here, for the sake of simplicity we have chosen to start with a surface profile of triangular shape. Owing to the fact that the dissolution slowness $L_{XZ}$ as given by Equation 4 remains unchanged when the angle $\theta$ takes successive values equal to $180° + \theta_1$ and $180° - \theta_1$ respectively, Figs 11 to 13 give the resultant $Z''$ dissolution profiles for the two faces of a given resonator. As expected the final shape of these dissolution profiles firstly, for a given cut varies from one face to another and secondly, for differently oriented quartz plates exhibits marked orientation effects.

When the numerical simulation is applied to the *Y* section of initial small radius (typical 12 $\mu$m we obtain the successive dissolution shapes illustrated in Fig. 14 which reflect the marked anisotropy of the dissolution process starting with an *Y* section of large radius (7.5 mm) we can calculate the out-of-roundness for the dissolution shapes of *Y* sections after selecting a reference circle from the least squares and then display a magnified profile graph (Fig. 15). Clearly this profile

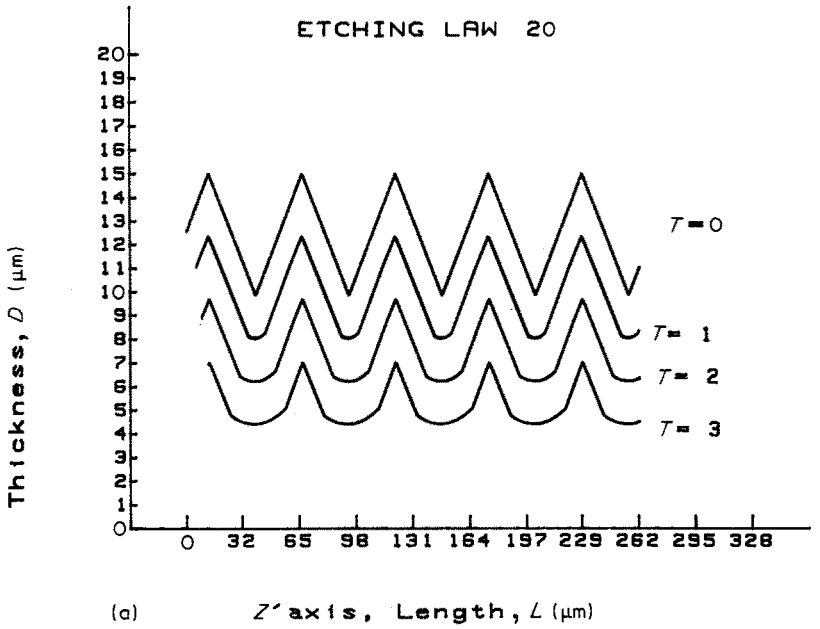


(a)

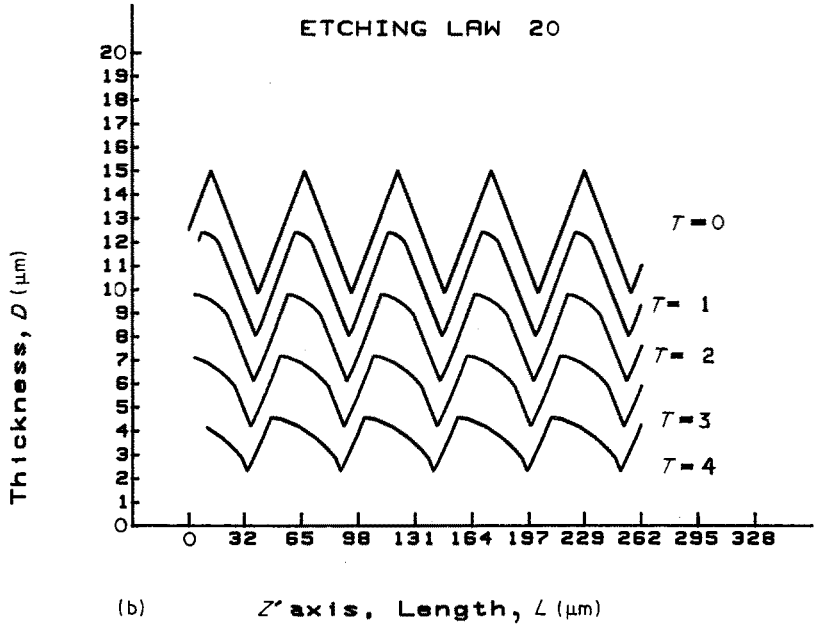


(b)

*Figure 13* As Fig. 11 for an *Y*-55 plate; (a) the planar face ($\theta$ = 55°); (b) the convex face ($\theta$ = 125°).

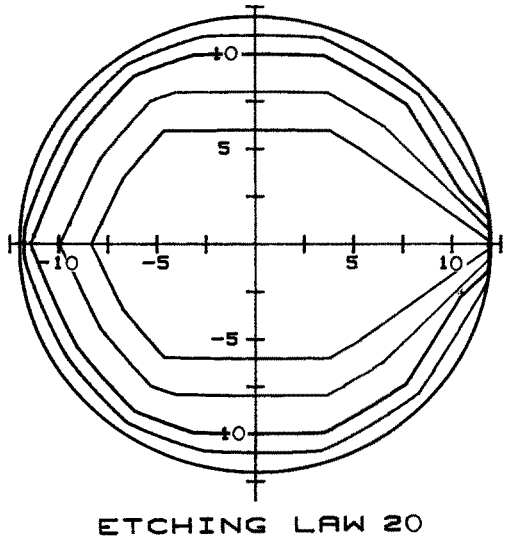


*Figure 14* The theoretical changes in the shape of an *Y* section with a starting circular shape.

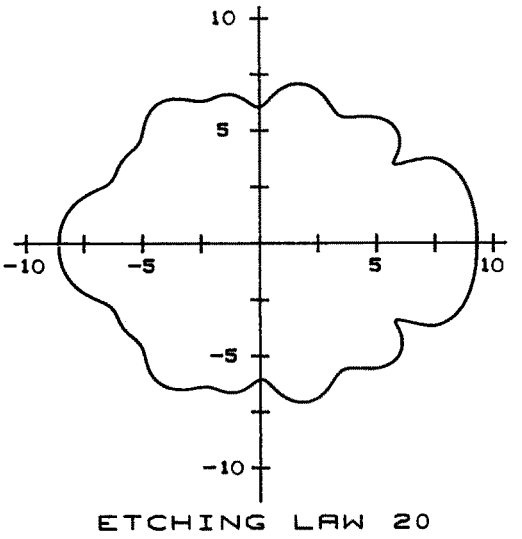


*Figure 15* The theoretical magnified graph of a deeply etched *Y* section.

TABLE I Comparison of experimental data on the etch rate, $R$, as determined from the Arrhenius plots of section with theoretical values as evaluated from the theoretical $Z''$ traces derived from the graphical simulation

| Plates | Experimental values of the etch rate $R$ ($nm\,sec^{-1}$) | Theoretical values of the dissolution rate $v_N(\theta)$ (arbitrary units) | Theoretical values of the average etch rate $R$ (arbitrary units) |
|---|---|---|---|
| Y-35 | Y-35-1 : R = 11<br>Y-35-2 : R = 11 | $\theta$ = 35° : 2.473<br>$\theta$ = 145° : 2.143 | 16.3 |
| Y-45 and Y*-45 | Y*-45-1 : R = 13 | $\theta$ = 45° : 1.803 | 13.6 |
| | Y-45-1 : R = 12.5 | $\theta$ = 145° : 2.604 | |
| Y-55 | Y-55-1 : R = 11<br>Y-55-2 : R = 11.5 | $\theta$ = 55° : 2.364<br>$\theta$ = 125° : 1.694 | 13.5 |

graph satisfies a mirror-like symmetry with respect to the $X$ axis.

## 5. Discussion and conclusion

Comparison of the magnified final $Z''$ profilometry traces made on the two faces of differently oriented $Y$-rotated plates (Fig. 5) with the theoretical final dissolution profiles (Figs 11 to 13) derived from the graphical simulation allows us to state that the proposed equation for the polar diagram of $L_{XZ}$ certainly represents quite accurately the dissolution slowness polar path related to $Y$-rotated plates whatever is the value of the angle $\theta$. Effectively, except for the convex $Y$-45 surface ($\theta$ = 135°) for which it is rather difficult to decide if the concavity of the $Z''$ profilometry traces is more accentuated than the convexity as predicted by Fig. 12b or vice versa, there is a clear correspondence between the shapes of the $Z''$ profilometry traces and theoretical $Z''$ profiles even for dissolution profiles of alternate concave–convex and convex–concave shapes.

We can also consider data on the etch rate. When the surface texture is produced by mechanical lapping the surface profile is characterized by a nearly Gaussian distribution of slopes corresponding to angles lying in the range $-15°$, $+15°$. Hence we have theoretically evaluated the depth of etch which is directly connected with the normal dissolution rate, $v_N$, starting from a triangular profile with slopes corresponding to $-15°$ and $+15°$, respectively. Repeating this procedure for all values of the angle into consideration in this study, allows us to infer, $R$, the average etch rate. The calculated values of $R$ as derived from the graphical simulation are reported in Table I where the corresponding data obtained in Section 3.1 are also shown for comparison. The scatter (less than 10%) between theoretical values is of the order of magnitude of the scatter between data indicating again that the maxima and the minima of $L_{XZ}(\theta)$ against $\theta$ are quite correctly positioned.

The third attempt to verify the agreement between theory and experiments which consists of considering simultaneously the experimental dissolution shape of Fig. 8 with the magnified theoretical dissolution profile shown in Fig. 14 appears also to be satisfactory. Recalling that, for orientations of the inward normal $\vec{n}$ close to the crystallographic $X$ axis, the deviation from the theoretical shape is associated with the initial procedure of indentification of the $X$ direction, it is obvious that the rest of the theoretical profile graph resembles to the experimental observation. In particular, there is a clear correspondence between values of the angle between the $X$ axis and the directions corresponding to peaks and valleys in the two profile graphs.

Thus we can really be hopeful that the various geometrical features (surface texture, shape of etched section) are consistently explained in terms of a tensorial representation of the dissolution slowness. We may conclude that Equation 5 is quite accurate to predict the etched shapes of $Y$-rotated quartz plates. This success encourages us to continue this relatively long work in order to determine all constants appearing in the general Equation 4 and to proceed in the future with a three-dimensional representation of dissolution shapes.

## References


1. J. R. VIG, W. WASSHAUSEN, C. COOK, M. KATZ and E. HAFNER, in Proceedings of the 27th Annual Symposium on Frequency Control, Fort Monmouth, New Jersey, 1973 (Electronic Industries Association, Washington, DC, 1973) p. 98.
2. J. R. WIG, J. W. LEBUS and R. FILLER, Report no. ECOM-4548 (US Army Electronics Research and Development Command, Fort Monmouth, New Jersey, 1977).
3. H. FUKUYO and N. OURA, in Proceedings of the 30th Annual Symposium on Frequency Control, Fort Monmouth, New Jersey, 1976 (Electronic Industries Association, Washington, DC, 1976) p. 254.
4. D. ANG in Proceedings of the 32nd Symposium on Frequency Control, Fort Monmouth, New Jersey, 1978 (Electronic Industries Association, Washington, DC, 1978) p. 282.
5. J. R. VIG, R. J. BRANDMAYR and R. L. FILLER, Report no. DELET-TR 80-5 (US Army Electronics Research and Development Command, Fort Monmouth, New Jersey, 1980).
6. R. J. BRANDMAYR and J. R. VIG, Report no. DELET-TR-81-16 (US Army Electronics Research and Development Command, Fort Monmouth, New Jersey, 1981).
7. C. R. TELLIER, *J. Mater. Sci.* **17** (1982) 1348.
8. *Idem, Surf. Technol.* **21** (1984) 83.
9. C. R. TELLIER and C. BURON, *ibid.* **22** (1984) 287.
10. C. R. TELLIER, in Proceedings of the 38th Annual Symposium on Frequency Control, Philadelphia, PA, 1984 (Institute of Electronic and Electrical Engineers, New York, 1984) p. 105.
11. *Idem*, in Proceedings of the XIth International Congress of Chronometry, Besançon, France, 1984 (Société Française des Microtechniques et de Chronométrie, Besançon, France, 1984) p. 115.
12. H. FUKUYO, N. OURA, N. KITAJIMA and H. KONO, *J. Appl. Phys.* **50** (1979) 3653.
13. J. R. VIG, C. F. COOK, K. SCHWIDTAL, J. W.

LEBUS and E. HAFNER, in Proceedings of the 28th Annual Symposium on Frequency Control, Fort Monmouth, New Jersey, 1974 (Electronic Industries Association, Washington, DC, 1974) p. 96.
14. C. R. TELLIER, C. BURON and F. JOUFFROY, *Mater. Chem. Phys.* **14** (1986) 25.
15. C. R. TELLIER and F. JOUFFROY, *J. Mater. Sci.* **18** (1983) 3621.
16. C. R. TELLIER in Proceedings of the 39th Annual Symposium on Frequency Control, Philadelphia, PA, 1985 (Institution of Electronic and Electrical Engineers, New York, 1985) p. 282.
17. M. CASTAGLIOLA, C. R. TELLIER and J. L. VATERKOWSKI, *J. Mater. Sci.* **21** (1986) 3551.
18. M. W. WEGNER and J. M. CHRISTIE, *Phys. Chem. Minerals* **9** (1983) 67.
19. R. B. HEIMANN, in "Silicon Chemical Etching", edited by J. Grabmaier (Springer, Berlin, 1982) p. 197.
20. A. P. HONESS, "The Nature, Origin and Interpretation of Etch Figures on Crystals" (Wiley, New York, 1927) Chapts III and VI.
21. K. H. YANG, *J. Electrochem. Soc.* **131** (1984) 1140.
22. C. R. TELLIER, N. VIALLE and J. L. VATERKOWSKI, in Proceedings of the 40th Annual Symposium on Frequency Control, Philadelphia, PA, 1986 (Institution of Electronic and Electrical Engineers, New York, 1986) p. 76.
23. *Idem*, in Proceedings of the 1st European Time and Frequency Forum, Besançon, France, 1987 (Imprimerie du Conseil Général du Doubs, Besançon, 1987) p. 159.
24. B. A. IRVING in "The Electrochemistry of Semiconductors" edited by P. J. Holmes (Academic Press, London, 1962) p. 256.
25. M. J. LIGHTHILL and G. B. WHITHAM, *Proc. Roy. Soc.* **A229** (1955) 281.
26. F. C. FRANK in "Growth and Perfection of Crystals" edited by R. H. Doremus, B. W. Roberts and D. Turnbull (John Wiley, New York, 1958) p. 411.
27. C. R. TELLIER, N. VIALLE and J. L. VATERKOWSKI, *Surf. Coatings Technol.* **34** (1988) 417.
28. C. R. TELLIER and J. L. VATERKOWSKI, *J. Mater. Sci.* **24** (1989) 1077.
29. P. VIGOUREUX and C. F. BOOTH, in "Quartz Vibrators and their Applications" (HMSO, London, 1950) Ch. 7.
30. H. EYRING and E. M. EYRING in "Modern Chemical Kinetics" (Reinhold, New York, 1965).
31. IEEE Standard on Piezoelectricity (Institution of Electronic and Electrical Engineers, New York, 1978) p. 15.

*Received 1 November*
*and accepted 18 November 1988*